

OPEN

SUBJECT AREAS:
SEISMOLOGY
GEOPHYSICSReceived
25 July 2014Accepted
2 October 2014Published
27 October 2014Correspondence and
requests for materials
should be addressed to
C.P. (pcy@geodevice.
cn)Early magnitude estimation for the $M_W7.9$ Wenchuan earthquake using progressively expanded P-wave time window

Chaoyong Peng, Jiansi Yang, Yu Zheng, Zhiqiang Xu & Xudong Jiang

Institute of Geophysics, China Earthquake Administration, No. 5 Minzudaxue South Road, Haidian District, Beijing 100081, China.

More and more earthquake early warning systems (EEWS) are developed or currently being tested in many active seismic regions of the world. A well-known problem with real-time procedures is the parameter saturation, which may lead to magnitude underestimation for large earthquakes. In this paper, the method used to the $M_W9.0$ Tohoku-Oki earthquake is explored with strong-motion records of the $M_W7.9$, 2008 Wenchuan earthquake. We measure two early warning parameters by progressively expanding the P-wave time window (PTW) and distance range, to provide early magnitude estimates and a rapid prediction of the potential damage area. This information would have been available 40 s after the earthquake origin time and could have been refined in the successive 20 s using data from more distant stations. We show the suitability of the existing regression relationships between early warning parameters and magnitude, provided that an appropriate PTW is used for parameter estimation. The reason for the magnitude underestimation is in part a combined effect of high-pass filtering and frequency dependence of the main radiating source during the rupture process. Finally we suggest only using P_d alone for magnitude estimation because of its slight magnitude saturation compared to the τ_c magnitude.

Earthquake Early Warning (EEW) systems have been researched and developed in Japan, Mexico, the United States, Taiwan, Italy, Turkey, and other countries^{1–12}. One of the important aspects of EEW is the rapid and reliable estimation of magnitude using the early portion of ongoing waveforms. In the last few years, several such techniques have been developed and implemented, based on empirical relationships between the event magnitude and parameters measured during the first seconds of the recorded signal. These early parameters are usually derived from the measure of *P*-phase frequency content^{13–16}, peak values^{17–20}, and integral quantities^{21,22}.

The $M_W7.9$ Wenchuan event represents an opportunity to check the extension of present EEW methodologies up to great earthquakes, to bring out their limits and to propose new strategies to overcome such limitations. For this earthquake, a dense strong-motion network deployed by China Strong Motion Network Center (CSMNC) provided seismic observations over a wide range of distances and azimuths from the source, with a high signal-to-noise ratio in the PTW up to several hundred kilometers from the source. This is the first time that a large number of ground motion records with such a high quality are obtained in China.

In this work we use two early warning parameters, the initial peak ground displacement (P_d) and the predominant period (τ_c) to get rapid estimations of the magnitude and to predict the potential damage of the earthquake. From the analysis of earthquakes in different regions of the world, several authors have found empirical relations between both these parameters and the earthquake size^{19,23–28} or between P_d and peak ground velocity (PGV) and acceleration (PGA)^{29,30}. However, these empirical relations were derived and validated using databases limited in magnitude up to 7–7.5^{14,15,30,31} and may not be suitable for great events. Furthermore these relationships are based on the analysis of the early *P*-wave signals of ground motion records in a 3- to 4-second time window. The saturation effect of early warning parameters with magnitude within this time window is well known and has been extensively discussed in the literature^{20,23,32,33}. Since the saturation is likely due to the use of only a few seconds of the *P*-wave which cannot capture the entire rupture process of a large earthquake²², we expect that longer PTWs are required to analyze large events^{34,35}. Another limitation is that the regression relationships among early warning parameters and source parameters have been generally applied up to 50–60 km of hypocentral distance, approximately covering the area in which the damaging effects of a moderate-to-large earthquake are expected.



Such a distance range is too restricted for the M_w 7.9 Wenchuan earthquake, which was felt as “strong” up to about 300 km. Finally, the acceleration data processing requires a high-pass filter to remove baseline effects caused by the double integration. While removing the artificial distortions, filters also reduce the low frequency content of the recorded waveforms and may change the scaling between early measurements and the final magnitude.

Here we want to investigate the reliability of existing early warning methodologies and empirical regression relations for the Wenchuan earthquake. In one literature, Hoshiba & Iwakiri³⁶ used strong-motion records of the 2011 Tohoku-Oki earthquake, and analyzed the initial peak ground motion and the τ_c parameter in the first 30 s after the first arrival at four accelerometric stations along the coast. Colombelli et al.³⁷ generalized this approach by expanding the analysis to larger PTW (up to 60 s) and epicentral distances (up to 530 km), showing that the early measurements of P_d and τ_c at the whole Japanese accelerometric network provided relevant insights on the ongoing earthquake rupture process and reliable estimations of the potential damage area. In this paper, the same method will be used to analyze strong-motion records of the Wenchuan earthquake which magnitude is one order smaller than the 2011 Tohoku-Oki earthquake, in order to check the validity of this method and whether there is saturation effect after applying this method to the Wenchuan earthquake strong-motion records. After taking into account the rupture length and the magnitude of this earthquake, we decide to use PTW with 30 s and fault distance within 200 km, not the epicentral distance.

Results

The Wenchuan earthquake occurred on May 15th, 2008 at 14:28:01 (Beijing Time). According to a study by the China Earthquake Administration (CEA), the earthquake occurred along the Longmenshan fault, a thrust structure along the border of the Indo-Australian Plate and Eurasian Plate. Seismic activities concentrated on its mid-fracture (known as Yingxiu-Beichuan fracture). The rupture lasted close to 120 sec, with the majority of energy released in the first 80 sec. Starting from Wenchuan, the rupture propagated at an average speed of 3.1 kilometers per second 49° toward north east, rupturing a total of about 300 km.

We analyzed 60, 3-component strong-motion accelerometer records for the Wenchuan earthquake, in the distance range between 0 and 200 km from the rupture. Waveforms were extracted from the CSMNC database. The sampling rates are 200 samples per second. Figure 1 shows the distribution of selected stations. We measured the initial peak displacement, P_d , and the predominant period, τ_c , after single and double integration to get velocity and displacement, respectively.

For real-time applications a causal 2-pole Butterworth, high-pass filter with a cut-off frequency of 0.075 Hz is usually applied to remove undesired long-period trends and baselines introduced by double integration³⁹. Zollo et al.³⁰ have shown that this cut-off frequency preserves a scaling of the early warning parameters with magnitude in a broad range ($4 < M < 7$). This frequency is lower or comparable to the corner frequency of any seismic event in the analyzed magnitude range, allowing to capture the low-frequency coherent radiation from the source. However, for great earthquakes the expected corner frequency is significantly smaller than such a cut-off filtering frequency. A preliminary study is then required to evaluate the effect of high-pass filtering on the Wenchuan earthquake records and of the expansion of the PTW.

We tested 110 combinations of cut-off frequencies and PTWs, from 0.001 Hz to 0.07 Hz and from 3 to 30 s, respectively. To avoid the S-wave contamination while increasing the PTW we computed the theoretical S-wave arrival times and excluded from our analysis all the stations for which the estimated S-wave arrival occurred within the considered PTW. While expanding the PTW the closest

stations are hence excluded one by one during the analysis. Furthermore, in order to compare the average P_d values for different stations, these have to be corrected for the geometrical attenuation effect. A global P_d -Magnitude scaling relationship obtained by Kuyuk & Allen²⁷ was used to correct the displacement for the distance effect and to normalize all the measured values to a reference distance of 100 km. In this research, they used data from earthquakes of magnitude 3.0–8.0 recorded in California and Japan. In addition, many events with magnitudes from 0.2 to 3.0 which were detected by the ElarmS EEWS from 1 May 2012 to 10 June 2013 were also used for obtaining the P_d -Magnitude relationship. These data set provides a “real world” view of the events that any EEWS must handle, i.e., very small earthquakes in addition to the larger magnitudes that the warning system is designed for. The best fit regression relationship for the global data set is

$$M_{GPD} = 1.23 \log(P_d) + 1.38 \log(R) + 5.39 \quad (1)$$

where M_{GPD} is the global P_d -Magnitude, R is the epicentral distance in kilometers and P_d is in centimeters. This relationship can also be rewritten into the following form in order to make it in the same format as those in previous studies:

$$\log(P_d) = 0.81 M_{GPD} - 1.12 \log(R) - 4.38 \quad (2)$$

Then we computed the average P_d and τ_c values as a function of the cut-off frequency for different PTWs. Results are shown in Figures 2 and 3. We found that both parameters vary with the cut-off frequency with a similar trend. Both P_d and τ_c assume the largest values for small cut-off frequencies and large PTWs. However, the relationships between these two parameters and the cut-off frequency for each considered PTW are gradually changed from linear to non-linear. For the parameters with PTW < 20 s, their logarithms decrease almost linearly with the cut-off frequency, but when the PTW expanding, the relationships are gradually changed into non-linear, especially for the parameters with the cut-off frequency < 0.01 Hz. The reason is that the epicentral distances for stations used for calculating the P_d and τ_c with PTW ≥ 20 s are more than 150 km and many other stations within 150 km are excluded. For these used stations the low-frequency content are more and more dominant in the data as the low cut-off frequency progressively decreases. This result is not consistent with that obtained by Combelle et al.³⁷ because most of the stations used in their study are located 150 km away from the epicentre and only data with PTW 30 s are used to calculate the two early parameters. If they use longer PTW, they should come to the same conclusion. However, from Figures 2 and 3 we can also find that there are linear regressions between these two parameters logarithms and the cut-off frequency for each considered PTW when the lower limit of the cut-off frequency is 0.02 Hz. This behavior suggests that, $\log(\tau_c)$ [or $\log(P_d)$] may be used for estimating the magnitude, provided that proper scaling coefficients are determined from the data with certain cut-off filtering frequency. For the sake of uniformity with the previous works and since the empirical relationships used in this work were obtained with a 0.075 Hz cut-off frequency, we decided to maintain this value for the filtering operation.

Using the procedure discussed above, we measured the early warning parameters using different PTWs, from 3 to 30 s for all the available records. Our aim is to understand whether the problem of magnitude underestimation due to parameter saturation may be overcome using appropriate PTWs and if the empirical regression relations relating early warning parameters and magnitude are still valid for this event. The saturation effect on P_d and τ_c measurements in short PTWs is well evident from data. Figures 4a and 4b show the mean value and standard deviation of P_d and τ_c within progressively increasing time windows measured after the first P -arrival. We again exclude data possible contaminated by the S-wave arrival and correct P_d estimates for the distance, according to equation (1). As for the

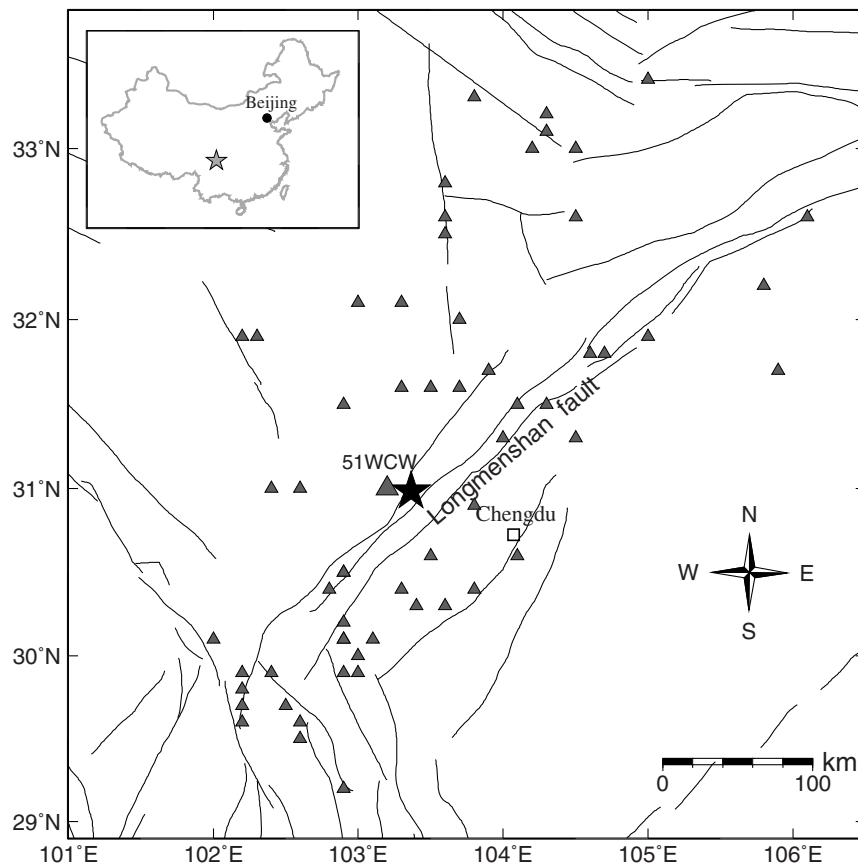


Figure 1 | Distribution of stations (triangles) used in this study with the closest station 51WCW shown as a larger size triangle. The black star represents the epicentre of the 2008 M_W 7.9 Wenchuan earthquake. The thin lines are faults described in Deng et al.³⁸. The star on the inset marks the study region in China. This figure is drawn using GMT software⁴⁹.

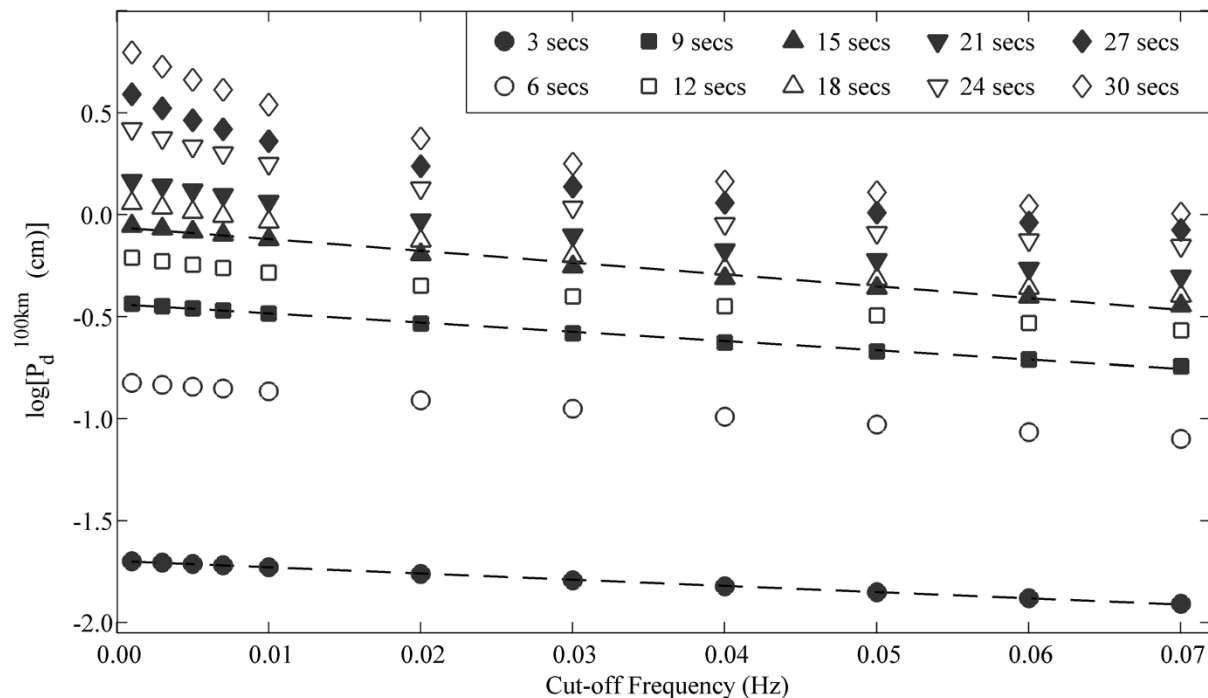


Figure 2 | Average values of P_d as a function of the cut-off frequency and of PTW. The dashed lines are the best fit curves evaluated through a linear regression on the P_d average values with PTW 3, 9, and 15 secs, respectively.

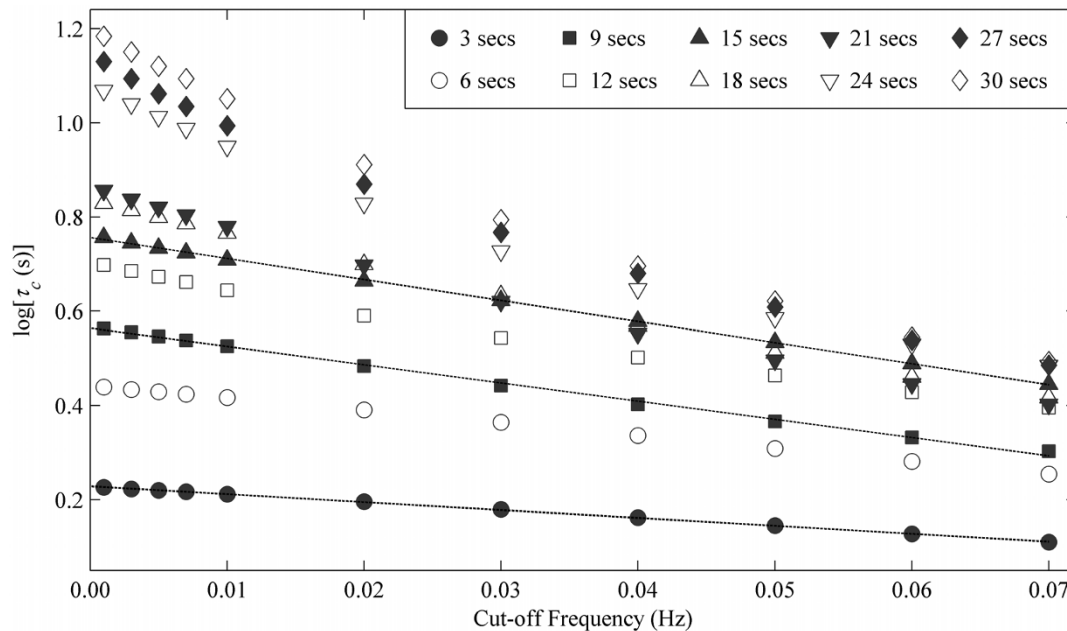


Figure 3 | Average values of τ_c as a function of the cut-off frequency and of PTW. The dashed lines are the best fit curves evaluated through a linear regression on the τ_c average values with PTW 3, 9, and 15 secs, respectively.

peak displacement (Figure 4a), it regularly increases with PTW, reaching a plateau at about 15–20 s, this corresponding to hypocentral distances greater than 100 km. From equation (1), the mean value of magnitude for $PTW \geq 20$ s is $M = 7.8 \pm 0.1$. The average period, τ_c (Figure 4b) shows a similar behavior although the errors on measurements at each PTW are much larger than those found for P_d . The average τ_c increases with PTW and becomes constant after 15–20 s at a mean value which corresponds to $M = 7.5 \pm 0.15$ according to the τ_c vs. M relationship²⁸. In both plots, error bars represent the standard deviation associated with each value; they depend not only on the scatter of the measurements but also on the number of observations, which decreases with increasing PTW. The final values of magnitude estimated from P_d and τ_c are consistent within error bars, suggesting that more robust estimations can be obtained by the combined use of amplitude and period parameters.

The available PTW at each time step and recording site depends on the P -wave propagation and on the apparent velocity through the seismic network. To use our approach in real-time early warning parameters, we reordered P_d and τ_c measurements as a function of time from the event Origin Time (OT), as it is usually done in early warning systems. We maintained the idea of the expanding PTW and, at the same time, we considered the delayed P -wave arrival time as a function of distance. In the previous analysis we used the same PTW for all the stations; here, instead, we use the maximum PTW available for each triggered station, i.e., the time interval between the observed P -wave arrival time and the theoretical S -wave arrival time. In this way all the stations contribute to the measurement, with shorter PTWs for nearby stations and longer PTWs for more distant stations. Results obtained from this analysis are plotted in Figure 5 (black circles) and show that the general trend of average P_d and τ_c is similar to that of Figure 4, both parameters providing evidence for saturation around 40 s from OT. A possible risk when averaging values resulting from windows with different lengths is that stations with short PTWs can provide a magnitude underestimation affecting the mean value. In order to reduce this effect, at each considered time step we computed weighted averages of P_d and τ_c with a weight proportional to the square of the window length (black triangles in Figure 5). However, with this approach we did not find any evident effect on the initial average values of P_d and τ_c being probably hidden by the larger variability of these two parameters obtained from only a

few of stations. In both cases, the final average magnitude values are gradually stable. For the case without weighting, the final magnitude values are 7.5 for P_d and 7.2 for τ_c after 40 s from OT, while for the weighted case the results are 7.6 for P_d and 7.3 for τ_c . Although there are some differences between these estimated magnitudes, the total trend is similar to the results of the previous analysis (Figure 4).

Beyond the real-time magnitude estimation another relevant goal of an EEW system is the rapid identification of the Potentially Damaged Zone (PDZ) and prompt broadcasting of a warning in the highest vulnerable areas before the arrival of the strongest shaking, so that security actions can be rapidly activated (i.e., automatic shut down of pipeline and gas line, ...). Following the same methodology as described in Colombelli et al.⁴⁰, and using the empirical scaling relationship of Zollo et al.³⁰ (equation 4), we estimated the P_d distribution for this earthquake, by interpolating the observed P_d values at close-in stations and the predicted P_d values at more distant sites. In Figure 6 we compare the Instrumental Intensity (I_{MM}) distribution (Figure 6a) with the predicted P_d distribution that would have been available 20 (Figure 6b), 30 (Figure 6c), 40 (Figure 6d), 50 (Figure 6e) and 60 s (Figure 6f) after the OT. The Instrumental Intensity distribution (Figure 6a) has been obtained from the observed Peak Ground Velocity at all the available stations, using the conversion table of Wald et al.⁴¹. In Figures 6b–6f, the stations for which measured values of P_d and τ_c are available are plotted with red and light blue triangles; the color represents the local alert level that would have been assigned to each recording site, following the scheme proposed by Zollo et al.³⁰. The alert levels can be interpreted in terms of potential damaging effects nearby the recording station and far away from it. For instance, an alert level 3 corresponds to an earthquake likely to have a large size and to be located close to the recording site, thus a high level of damage is expected both nearby and far away from the station. The PDZ of Figure 6b is fairly consistent with the area where the highest intensity values are observed (i.e., $I_{MM} > 7$). Although the first reliable mapping of the P_d distribution is available 20 s after OT, the local alert levels at the stations are available well before (two alert level 3 at the closest stations are available 12 s after the OT); this information can be used to issue a warning, despite the magnitude estimation has not yet reached its final value. A stable P_d distribution is finally available later in time, around 40 s after OT (Figure 6d). However, in the north-east part of

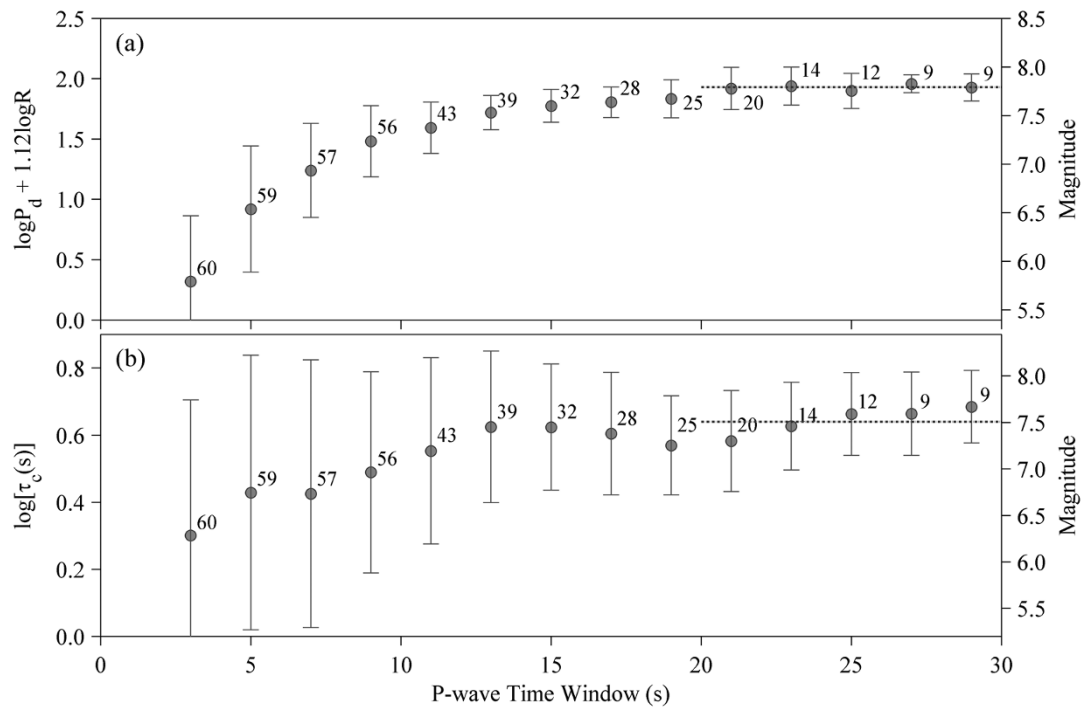


Figure 4 | Average values of (a) P_d and (b) τ_c as a function of the P -wave Time Window used. Error bars are computed as the standard deviation associated to each value; the gray number close to each point represents the number of stations used for each considered time window. Both parameters exhibit saturation when a 10–20 s PTW is used. The final saturation level (PTW ≥ 20 s) is shown by the gray dotted lines. For each plot, the corresponding magnitude scale is also represented; this has been derived based on the coefficients of equation (1) and on the τ_c vs. M relationship determined by Peng et al.²⁸.

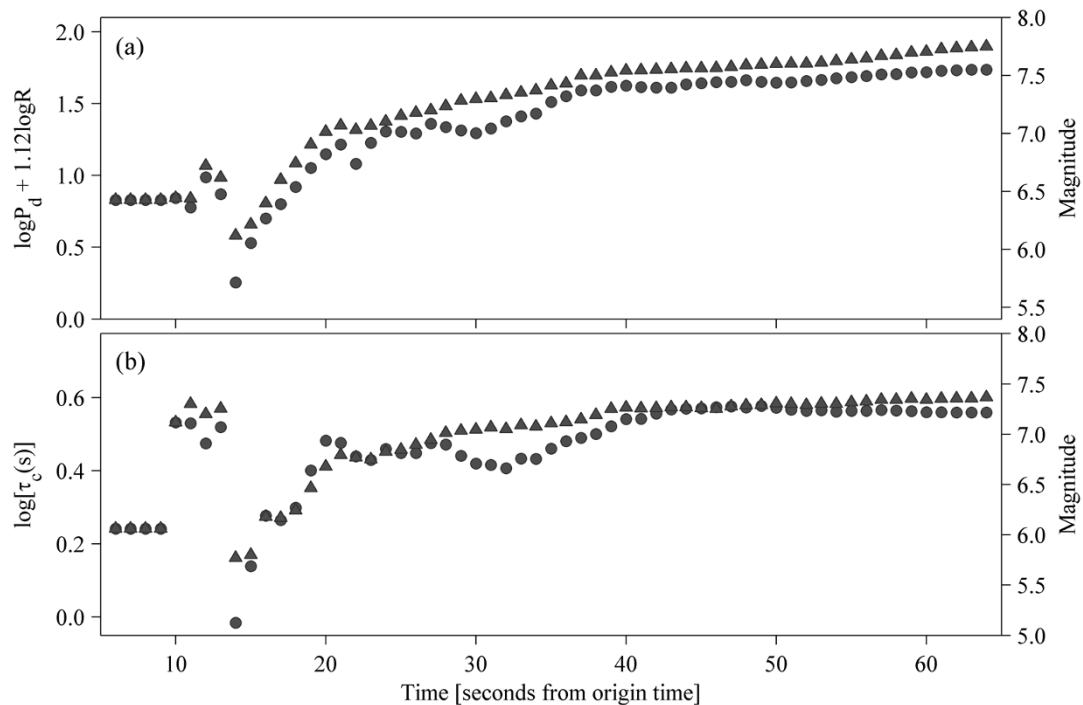


Figure 5 | Real-time evolution of (a) P_d and (b) τ_c as a function of time from the origin time. In each plot, circles represent the standard average values while triangles are the result of the weighted average computation. Each weight is proportional to the square of the PTW, so that the longer the available record, the more relevant the contribution to the computation. For each plot, the corresponding magnitude scale is also represented; this has been derived based on the coefficients of equation (1) and on the τ_c vs. M relationship determined by Peng et al.²⁸.

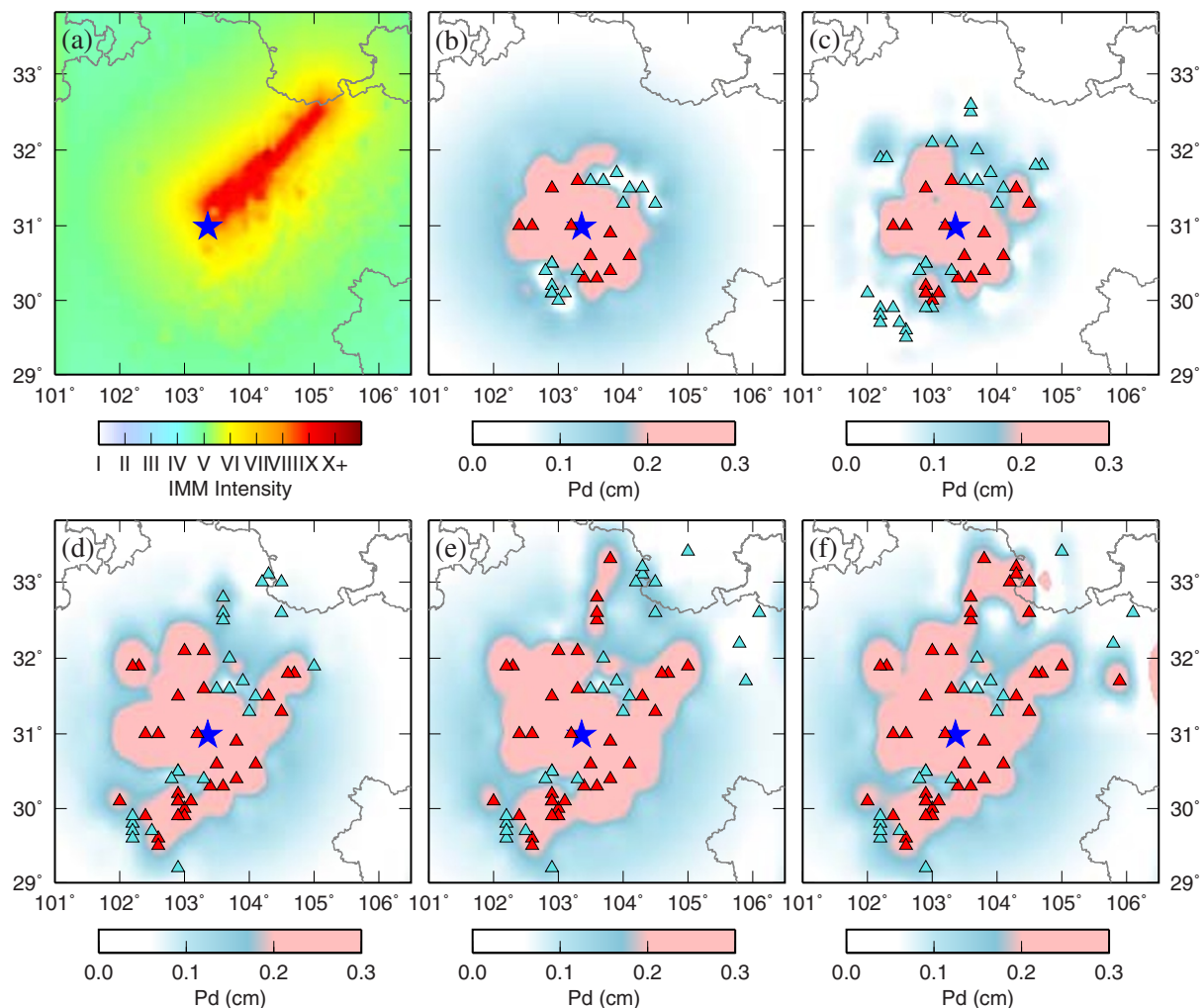


Figure 6 | Comparison between (a) the real Instrumental Intensity (I_{MM}) distribution and the predicted P_d distribution that would have been available (b) 20, (c) 30, (d) 40, (e) 50, and (f) 60 s after the OT. The Instrumental Intensity distribution (Figure 6a) has been performed by USGS⁴¹ and is downloaded from its website (<http://earthquake.usgs.gov/earthquakes/shakemap/global/shake/2008ryan/>). Figures 6b–6f show the distribution of P_d values, obtained after interpolating measured and predicted initial displacement values. The color transition from light blue to red represent the $P_d = 0.2$ cm isoline, which corresponds to a $I_{MM} = 7$, based on the scaling relationship of equation (1) in Zollo et al.³⁰. The available stations at each time are plotted with red and light blue triangles, based on the local alert level. The blue star represents the epicentre of the 2008 M_W 7.9 Wenchuan earthquake. This figure is drawn using GMT software⁴⁹.

Sichuan province the intensity values are not well reproduced, probably due to the sparse distribution of strong-motion stations.

Discussion

Although the complexity of the rupture process for large earthquakes has not yet been fully understood, the application of early warning methodologies to the Wenchuan strong-motion records can represent a useful tool to reveal new insights into the very delicate issue of early magnitude estimation for large earthquakes and the prediction of the potential damage area while the rupture process is still ongoing. The analysis performed in this work provided relevant implications for both the physical properties of the seismic source and the more practical aspects related to the implementation of real-time early warning methodologies for large events.

As for the first aspect, the evolutionary estimation of P_d and τ_c as a function of the PTW showed that the existing methodologies and regression relationships commonly used for early warning applications can be extended even to this large earthquake, provided that appropriate time and distance windows are selected for the measurements. We found that P_d and τ_c are indeed largely underestimated when a small PTW (a few seconds) is used while stable and consistent

values are obtained for PTW exceeding 15–20 s. It has to be noted that, although the average values are well consistent, the strong variability of τ_c makes the uncertainties on this parameter at each PTW much larger than those on P_d . The scaling between these two early warning parameters and the magnitude remains the same as for $M < 7$ earthquakes, allowing for a correct real-time evaluation of the event size.

This study adopts the same method of Colombelli et al.⁴⁰ which extended the analysis of Hoshiba & Iwakiri³⁶, by overcoming the limitation owing to the use of the closest four accelerometric stations along the coast (at a maximum epicentral distance of 164 km). For such stations the S-waves are expected to arrive within the selected 30 s time window and their inclusion within the PTW may introduce a significant bias in magnitude estimations because of a different scaling between magnitude and early warning parameters for P- and S-waves^{19,42}. Furthermore, the limited distance range analyzed by Hoshiba & Iwakiri³⁶ is expected to provide a partial image of the ongoing source process, whose full investigation requires broader time and distance/azimuth ranges. We came to the conclusion that both P_d and τ_c estimate an earthquake magnitude $M \geq 7.5$ when using large PTWs (>20 s), although uncertainties in magnitude



estimation from P_d (~ 0.2) are significantly smaller than the uncertainties from τ_c (~ 0.5).

As for the magnitude estimation of Wenchuan earthquake with real-time processing, P_d and τ_c exhibit a saturation effect and provide a magnitude estimation of $M = 7.6$ and $M = 7.3$, respectively. Since the final earthquake magnitude is $M_W 7.9$, does this smaller value reflect the magnitude of the early portion of the event or is it an artifact due to uncertainties in the empirical regression laws and/or to measurement procedures? Kinematic inversions for this earthquake have shown a complex frequency dependent rupture history, with asperities radiating energy with different frequency content at different locations. The moment rate function⁴³ can be used as a proxy for the far-field P -wave displacement if the finite fault effects such as directivity and changes in the focal mechanism are neglected. The whole time history of the mainshock is divided into five stages, that is, consists of five sub-events⁴³. The first event occurred in the first 14 s after the rupture initiation, releasing 14% of the total scalar seismic moment. The second event, the main event, was from 14 s to 34 s, releasing 60% of the total scalar seismic moment. The third one started at 34 s and ended at 43 s, releasing 8% of the total scalar seismic moment. The fourth occurred in the time period of 43 s to 58 s, releasing 17% of the total scalar seismic moment. And the last one started at 58 s, and ruptured weakly until the end of the whole rupture process (90 s), releasing only 6% of the total scalar seismic moment. The saturation observed in the P_d vs. PTW plot (Figure 4a) beyond 13 s probably corresponds to the end of the first rupture episode. Since the second rupture episode appears to be deficient in high-frequency (>0.05 Hz) energy radiation, we therefore suggest that the 0.075 Hz high-pass filter used for the evolutionary estimation of P_d and τ_c captured the energy from the first event while filtering out the prominent energy emitted from the second one, thus leading to a smaller magnitude, 7.5 (Figure 4b), when compared to the final earthquake size. However, consistency of P_d and τ_c (Figures 4a and 4b) with the shape of moment rate time function of Zhang et al.⁴³ in the initial 14 s of rupture suggests that early warning parameters provide an evolutionary image of the ongoing fracture process.

Despite of the final magnitude underestimation we note that, for the Wenchuan earthquake, the high-pass filtering did not prevent a correct evaluation of the PDZ. The prediction of the PDZ becomes stable about 40 s after the OT. This study suggests that records at distances up to several hundred kilometers from the earthquake epicentre help in constraining the magnitude estimation obtained from near-source data. However, the maximum distance to be considered needs to be properly defined as a function of the signal-to-noise ratio, which decreases with epicentral distance and event size. Automatic selection of the proper PTW can be achieved, for example, by increasing the PTW until both P_d and τ_c parameters stabilize, i.e., until no significant variations are observed. In order to account for the uncertainties on P_d and τ_c , appropriate strategies to combine these two parameters could be adopted, such as Bayesian probabilistic approaches as proposed by Lancieri & Zollo⁴⁴, or we can only use P_d alone for magnitude estimation because its uncertainties are smaller than those of τ_c and the final estimated event size is closer to $M_W 7.9$ than the magnitude size for τ_c . Furthermore, an initial location of the hypocentre is required, in order to correctly estimate the S -wave arrival time, and to exclude data at stations for which the S -waves are expected to arrive within the selected PTW. For this, we can use the RTLoc location algorithm which is proposed by Satriano et al.⁴⁵ and based on the equal differential time (EDT) formulation⁴⁶ and on a fully probabilistic description of the hypocentre. This method is able to provide with a first, approximate epicentral location by using just one station, applying the concept of Voronoi cells^{45,47}. As far as new P picks are available, a probabilistic, evolutionary estimation of epicentre, depth and origin time is obtained, with improved accuracy.

The proposed evolutionary approach based on gradually increasing PTWs provides, for the Wenchuan earthquake, stable magnitude estimations within 35–40 s after the OT. The availability of real-time measurements of P_d and τ_c at the closest stations allows for a rapid prediction of the expected ground motion at stations located far away from the source area and for a rapid estimation of the PDZ. For Beichuan County where 20,000 residents were declared dead or missing, nearly accounting for one-quarter of the overall death toll from the catastrophe, this information would have been released approximately 10 seconds before the Beichuan fault started to rupture. Thus, longer PTWs would have not diminished the usefulness for early warning in this case.

Methods

The automatic P first arrival picking method described by Allen⁴⁸ is used to detect the P wave arrival from the vertical record. The offset of the vertical-component accelerometer is corrected by subtracting the mean of the early portion of the data to obtain $u_d(t)$. It is integrated, passed through a second-order one-way high-pass Butterworth filter of 0.075 Hz for removing the low-frequency drift after the integration process, and integrated and filtered again to obtain the displacement waveforms, $u_d(t)$. The displacement is then differentiated to obtain the velocity, $u_v(t)$. The peak amplitude P_d is the maximum absolute amplitude of $u_d(t)$ for the range between t_p and $t_p + t_N$, where t_p is the P -wave onset time. For t_N , it starts from 3 s to the time T_{S-P} . The parameter τ_c is obtained from

$$\tau_c = 1/\sqrt{\langle f^2 \rangle} = \sqrt{\int_0^\infty |U_d(f)|^2 df / \int_0^\infty f^2 |U_d(f)|^2 df} \quad (3)$$

$$= 2\pi \sqrt{\int_{t_p}^{t_p+t_N} u_d^2(t) dt / \int_{t_p}^{t_p+t_N} u_v^2(t) dt},$$

where f and $U_d(f)$ are the frequency and the frequency spectrum of $u_d(t)$, respectively, and $\langle f^2 \rangle$ is the average of f^2 weighted by $|U_d(f)|^2$.

- Hoshiba, M., Kamigaichi, O., Saito, M., Tsukada, S. & Hamada, N. Earthquake early warning starts nationwide in Japan. *EOS Trans. Am. Geophys. Union* **89**, 73–74 (2008).
- Alcik, H., Ozel, O., Apaydin, N. & Erdik, M. A study on warning algorithms for Istanbul earthquake early warning system. *Geophys. Res. Lett.* **36**(L00B05) (2009).
- Allen, R. M. et al. Real-time earthquake detection and hazard assessment by ElarmS across California. *Geophys. Res. Lett.* **36**(L00B08) (2009).
- Espinosa-Aranda, J. M. et al. Evolution of the Mexican Seismic Alert System (SASMEX). *Seism. Res. Lett.* **80**, 694–706 (2009).
- Hsiao, N. C., Wu, Y. M., Shin, T. C., Zhao, L. & Teng, T. L. Development of earthquake early warning system in Taiwan. *Geophys. Res. Lett.* **36**(L00B02) (2009).
- Kamigaichi, O. et al. Earthquake Early Warning in Japan—Warning the general public and future prospects—. *Seismol. Res. Lett.* **80**, 717–726 (2009).
- Nakamura, H., Horiuchi, S., Wu, C., Yamamoto, S. & Rydelek, P. A. Evaluation of the real-time earthquake information system in Japan. *Geophys. Res. Lett.* **36**(L00B01) (2009).
- Zollo, A. et al. Earthquake early warning system in southern Italy: Methodologies and performance evaluation. *Geophys. Res. Lett.* **36**(L00B07) (2009).
- Satriano, C. et al. PRESTo, the earthquake early warning system for Southern Italy: concepts, capabilities and future perspectives. *Soil Dyn. Earthqu. Eng.* **31**, 137–153 (2011).
- Peng, H. S. et al. Developing a prototype earthquake early warning system in the Beijing capital region. *Seismol. Res. Lett.* **82**, 394–403 (2011).
- Carranza, M., Buform, E., Colombelli, S. & Zollo, A. Earthquake early warning for southern Iberia: A P wave threshold-based approach. *Geophys. Res. Lett.* **40**, 4588–4593 (2013).
- Reza, H., Shomali, Z. H. & Ghayamghamian, M. R. Magnitude-scaling relations using period parameters τ_c and τ_p^{\max} , for Tehran region, Iran. *Geophys. J. Int.* **192**, 275–284 (2013).
- Nakamura, Y. On the urgent earthquake detection and alarm system (UrEDAS). In *Proceedings of the Ninth World Conference on Earthquake Engineering*, Tokyo-Kyoto, Japan, volume VII, 673–678 (1988).
- Allen, R. M. & Kanamori, H. The potential for early warning in Southern California. *Science* **300**, 786–789 (2003).
- Wu, Y. M. & Kanamori, H. Experiment of an on-site method for the Taiwan Early Warning System. *Bull. Seismol. Soc. Am.* **95**, 347–353 (2005).
- Simons, F. J., Dando, B. D. E. & Allen, R. M. Automatic detection and rapid determination of earthquake magnitude by wavelet multiscale analysis of the primary arrival. *Earth Planet. Sci. Lett.* **250**, 214–223 (2006).
- Wu, Y. M. & Zhao, L. Magnitude estimation using the first three seconds P -wave amplitude in earthquake early warning. *Geophys. Res. Lett.* **33**(L16312) (2006).



18. Wu, Y. M., Kanamori, H., Allen, R. M. & Hausson, E. Determination of earthquake early warning parameters, τ_c and P_d , for southern California. *Geophys. J. Int.* **170**, 711–717 (2007).
19. Zollo, A., Lancieri, M. & Nielsen, S. Earthquake magnitude estimation from peak amplitudes of very early seismic signals on strong motion records. *Geophys. Res. Lett.* **33**(L23312) (2006).
20. Zollo, A., Lancieri, M. & Nielsen, S. Reply to comment by P. Rydelek et al. on “Earthquake magnitude estimation from peak amplitudes of very early seismic signals on strong motion records” *Geophys. Res. Lett.* **34**(L20303) (2007).
21. Böse, M., Wenzel, F. & Erdik, M. Preseis: A neural network-based approach to earthquake early warning for finite faults. *Bull. Seismol. Soc. Am.* **98**, 366–382 (2008).
22. Festa, G., Zollo, A. & Lancieri, M. Earthquake magnitude estimation from early radiated energy. *Geophys. Res. Lett.* **35**(L22307) (2008).
23. Kanamori, H. Real-time seismology and earthquake damage mitigation. *Annu. Rev. Earth Planet. Sci.* **33**, 195–214 (2005).
24. Böse, M., Ionescu, C. & Wenzel, F. Earthquake early warning for Bucharest, Romania: Novel and revised scaling relations. *Geophys. Res. Lett.* **34**(L07302) (2007).
25. Wu, Y. M. & Kanamori, H. Development of an earthquake early warning system using real-time strong motion signals. *Sensors* **8**, 1–9 (2008).
26. Shieh, J. T., Wu, Y. M. & Allen, R. M. A comparison of τ_c and τ_p^{max} for magnitude estimation in earthquake early warning. *Geophys. Res. Lett.* **35**(L20301) (2008).
27. Kuyuk, H. S. & Allen, R. M. A global approach to provide magnitude estimates for earthquake early warning alerts. *Geophys. Res. Lett.* **40**, 6329–6333 (2013).
28. Peng, C. Y., Yang, J. S., Xue, B., Zhu, X. Y. & Chen, Y. Exploring the feasibility of earthquake early warning using records of the 2008 Wenchuan earthquake and its aftershocks. *Soil Dyn. Earthqu. Eng.* **57**, 86–93 (2014).
29. Wu, Y. M. & Kanamori, H. Rapid assessment of damaging potential of earthquakes in Taiwan from the beginning of P waves. *Bull. Seismol. Soc. Am.* **95**, 1181–1185 (2005).
30. Zollo, A., Amoroso, O., Lancieri, M., Wu, Y. M. & Kanamori, H. A threshold-based earthquake early warning using dense accelerometer networks. *Geophys. J. Int.* **183**, 963–974 (2010).
31. Olson, E. L. & Allen, R. M. The deterministic nature of earthquake rupture. *Nature* **438**, 212–215 (2005).
32. Rydelek, P. & Horiuchi, S. Is earthquake rupture deterministic? *Nature* **443**, E5–E6 (2006).
33. Rydelek, P., Wu, C. & Horiuchi, S. Comment on “Earthquake magnitude estimation from peak amplitudes of very early seismic signals on strong motion records” by Aldo Zollo, Maria Lancieri, and Stefan Nielson. *Geophys. Res. Lett.* **34**(L20302) (2007).
34. Lomax, A. & Michelini, A. Mwpd: A duration-amplitude procedure for rapid determination of earthquake magnitude and tsunamigenic potential from P waveforms. *Geophys. J. Int.* **176**, 200–214 (2009).
35. Bormann, P. & Saul, J. Earthquake magnitude. In Meyers, R. editors, *Encyclopedia of Complexity and Systems Science*, pages 2473–2496. Springer (2009).
36. Hoshiba, M. & Iwakiri, K. Initial 30 seconds of the 2011 off the Pacific coast of Tohoku Earthquake (M_W 9.0)—amplitude and τ_c for magnitude estimation for Earthquake Early Warning—. *Earth Planet. Sci.* **63**, 553–557 (2011).
37. Colombelli, S., Zollo, A., Festa, G. & Kanamori, H. Early magnitude and potential damage zone estimates for the great M_W 9 Tohoku-Oki earthquake. *Geophys. Res. Lett.* **39**(L22306) (2012).
38. Deng, Q. D. et al. Basic characteristics of active tectonics of China. *Sci. China Ser. D-Earth Sci.* **46**, 356–372 (2003).
39. Boore, D. M., Stephens, C. D. & Joyner, W. B. Comments on baseline correction of digital strong-motion data: Examples from the 1999 Hector Mine, California, earthquake. *Bull. Seismol. Soc. Am.* **92**, 1543–1560 (2002).
40. Colombelli, S., Amoroso, O., Zollo, A. & Kanamori, H. Test of a threshold-based earthquake early warning using Japanese data. *Bull. Seismol. Soc. Am.* **102**, 1266–1275 (2012).
41. Wald, D. J., Quitoriano, V., Heaton, T. H. & Kanamori, H. Relationships between peak ground acceleration, peak ground velocity and modified Mercalli intensity in California. *Earthquake Spectra* **15**, 557–564 (1999).
42. Peng, C. Y., Yang, J. S., Xue, B., Chen, Y. & Zhu, X. Y. Research on correlation between early-warning parameters and magnitude for the Wenchuan Earthquake and its aftershocks. *Chinese J. Geophys.-CH.* **56**, 3404–3415 (2013).
43. Zhang, Y., Feng, W. P., Xu, L. S., Zhou, C. H. & Chen, Y. T. Spatio-temporal rupture process of the 2008 great Wenchuan earthquake. *Sci. China Ser. D-Earth Sci.* **52**, 145–154 (2009).
44. Lancieri, M. & Zollo, A. A Bayesian approach to the real time estimation of magnitude from the early P- and S-wave displacement peaks. *J. Geophys. Res.* **113**(B12302) (2008).
45. Satriano, C., Lomax, A. & Zollo, A. Real-time evolutionary earthquake location for seismic early warning. *Bull. Seismol. Soc. Am.* **98**, 1482–1494 (2008).
46. Font, Y., Kao, H., Lallemand, S., Liu, C.-S. & Chiao, L.-Y. Hypocentral determination offshore Eastern Taiwan using the Maximum Intersection method. *Geophys. J. Int.* **158**, 655–675 (2004).
47. Cua, G. & Heaton, T. The virtual seismologist (VS) method: a Bayesian approach to earthquake early warning. In *Earthquake Early Warning Systems*; Gasparini, P., Manfredi, G., and Zschau, J., editors, 97–132 (2007).
48. Allen, R. V. Automatic earthquake recognition and timing from single traces. *Bull. Seismol. Soc. Am.* **68**, 1521–1532 (1978).
49. Wessel, P. & Smith, W. H. F. New, improved version of generic mapping tools released. *Eos Trans. AGU* **79**, 579 (1998).

Acknowledgments

We greatly appreciate Alessio Piatanesi for his very constructive suggestions, which helped improve the manuscript. We also thank China Strong Motion Networks Center for providing acceleration seismograms of the Wenchuan mainshock (<http://www.csmnc.net/>). This research was supported by the National Natural Science Foundation of China (41404048). Research was also partially funded by the Seismological Research Project 201108002 and the National Key Technologies R&D Program of the Ministry of Science and Technology of the People's Republic of China 2012BAF14B12.

Author contributions

C.P. processed the strong-motion data and prepared the manuscript. J.Y. has contributed to the revision of this paper and provided insightful comments and suggestions. Y.Z., Z.X. and X.J. provided important suggestions on the offline test and article revision. All authors reviewed the manuscript.

Additional information

Competing financial interests: The authors declare no competing financial interests.

How to cite this article: Peng, C., Yang, J., Zheng, Y., Xu, Z. & Jiang, X. Early magnitude estimation for the M_W 7.9 Wenchuan earthquake using progressively expanded P-wave time window. *Sci. Rep.* **4**, 6770; DOI:10.1038/srep06770 (2014).



This work is licensed under a Creative Commons Attribution-NonCommercial-NoDerivs 4.0 International License. The images or other third party material in this article are included in the article's Creative Commons license, unless indicated otherwise in the credit line; if the material is not included under the Creative Commons license, users will need to obtain permission from the license holder in order to reproduce the material. To view a copy of this license, visit <http://creativecommons.org/licenses/by-nc-nd/4.0/>



DOI: 10.1038/srep07602

SUBJECT AREAS:
SEISMOLOGY
GEOPHYSICS

RETRACTION: Early magnitude estimation for the $M_W 7.9$ Wenchuan earthquake using progressively expanded P-wave time window

Chaoyong Peng, Jiansi Yang, Yu Zheng, Zhiqiang Xu & Xudong Jiang

SCIENTIFIC REPORTS:
4 : 6770
DOI: 10.1038/srep06770
(2014)

The authors wish to retract this Article because large sections of the text were copied from a Colombelli *et al.* study, which was cited as reference 37. The results and data presented in the Article have not been contested.

Published:
27 October 2014

Updated:
16 January 2015